Oil Shale, 2026, 43, 2, 165–196 https://doi.org/10.3176/oil.2026.2.03

Optimization of oil shale retorting process based on heat transfer model

Chunhua Wang[(a)]*, Yufeng Wu[(a)], Chunhui Wang[(b)], Ningning Li[(a)]*, Lina Liu[(a)], Chengdong He[(a)], Jiang Liu[(a)], Yue Yue[(a)], Haodan Pan[(a)], Zhiyong Hu[(c)], Yulin Yan[(d)]

[(a)] College of Mechanical Engineering, Liaoning Petrochemical University, Fushun 113001, China
[(b)] China National Energy Group Ledong Power Generation Co. Ltd., Ledong 572539, China
[(c)] College of Petroleum Engineering, Liaoning Petrochemical University, Fushun 113001, China
[(d)] Fushun Mining Group Co. Ltd., Fushun 113009, China

Received 8 February 2025, accepted 8 April 2026, available online 16 April 2026

Abstract. *To optimize the oil shale retorting process and improve the thermal efficiency of the retort, a heat transfer model of the oil shale retorting in the Fushun-type retort was established based on the gas-solid heat transfer equation. The orthogonal experimental method was used, with hot air volume (A), hot recycle gas temperature (B), and oil shale interparticle porosity (C) taken as the investigation factors, and the retort height required for the retorting of the same quality oil shale as the metric of the thermal efficiency of the retort. The smaller the retort height, the higher the thermal efficiency of the retort. Range and variance analyses revealed that the effects of the three factors on retort height are, from large to small: A > B >C; this shows that hot air volume (A) exerts the most significant influence. Based on this, computational fluid dynamics simulation was conducted on the hot air volume parameter. The study shows that increasing the hot air volume can effectively increase the heat supply proportion of the generated gas in the retorting process to 59.288%. To maintain the height of the high-temperature zone in the reaction section, it is proposed to increase the oxygen content in the hot air volume, which proves the feasibility of oxygen-enriched retorting.*

Keywords: *oil shale retorting, heat transfer model, orthogonal experimental, hot air volume.*

* Corresponding authors, wangchunhua@lnpu.edu.cn, lining773239@163.com

1. Introduction

Oil shale is a kerogen-rich sedimentary rock that can be broken down when heated to produce shale oil and pyrolysis gas. Its global reserves far exceed those of traditional oil, making it a valuable energy resource for countries such as the United States, Russia, and China. Oil shale under air-isolated conditions can be subjected to low-temperature retorting to obtain shale oil, shale semi-coke, and pyrolysis gas. Among the existing ground-based retorting processes for industrial production, the gas heat-carrier retorting process is the most widely used, such as Brazil's Petrosix process, Estonia's Kiviter process, the U.S. SGR process, Japan's Joseco process, and China's Fushun retorting process. The Fushun-type retort is equipment for oil shale retorting that uses hot recycle gas as a heat carrier, and it has achieved the largest commercial production in China [1].

Many operating parameters affect the thermal efficiency of oil shale retorting. Many scholars have analyzed the effects of typical parameters on the retorting process of oil shale, including heating rates, grain size of oil shale, pyrolysis process temperature, and residence time of oil shale. Wang et al. [2, 3] investigated the effects of different heating rates on the density, viscosity, boiling point, cloud point, and calorific value of shale oil during pyrolysis of oil shale. Nazzal [4] showed that shale oil coking at higher heating rates leads to lower yields. This may be because the temperature difference between the core and oil shale surface increases significantly as the heating rate rises during the pyrolysis process. Geng et al. [5] found that the shale oil yield increases significantly during oil shale pyrolysis at temperatures ranging from 300 to 500 °C and decreases above 500 °C due to the enlargement of oil shale pores and secondary decomposition of pyrolysis products. Pan et al. [6] conducted a similar study. The results demonstrate that oil shale yield is positively correlated with temperatures from 350 to 520 °C and negatively correlated at temperatures ranging from 520 to 600 °C. Experiments by Xu et al. [7] showed that increasing the residence time can improve the physical properties of oil shale, but a residence time that is too long can lead to secondary decomposition of oil and gas. Han et al. [8] used gas chromatography–mass spectrometry to extract and characterize the organic compounds in shale coke under different pyrolysis conditions. A prolonged residence time leads to the enrichment of aromatic hydrocarbons and nitrogenous organic compounds in oil shale coke, resulting in lower shale oil grades. Khalil [9] indicated that the particle size of oil shale affects mass transfer, heat transfer, and secondary reactions during pyrolysis, and that an increase in particle size leads to a decrease in total weight loss and gas weight loss, as well as a decrease in the amount of oil produced. Tang [10] conducted a study on samples with different grain sizes and performed thermogravimetric analysis. These results are consistent with those of previous assessments. However, in the oil shale retorting process, the influence of relevant operating parameters on the retort's thermal efficiency remains poorly understood.

Moreover, it is unclear which of these parameters have the most significant impact and which can be neglected.

Therefore, a numerical heat transfer model was established for oil shale retorting in the Fushun-type retort based on the gas-solid heat transfer equation in this work. The specific effects of the three typical parameters – hot air volume, hot recycle gas temperature, and oil shale interparticle porosity – on the heat utilization efficiency of the retort were discussed, the key factors affecting the thermal efficiency of the retort were determined, and effective improvement measures to improve the thermal efficiency of the retort were proposed.

2. Research object and methods

2.1. Research object

The Fushun-type retort can be divided into three sections from top to bottom [11]: drying, retorting, and gasification sections, as shown in Figure 1. The process flow for each section is as follows:

(1) Drying section

Oil shale with a particle size between 12 and 75 mm is fed into the retort from the top via the feeding device and then enters the drying section, flowing in a top-down direction. In the drying section, the oil shale comes into counter-current contact with the upward-flowing shale oil and gas mixture. It is heated to a temperature of 100–150 °C, causing the moisture within it to be released. The released moisture rapidly evaporates into steam and mixes with the oil and gas mixture, thus completing the drying process. Subsequently, the shale oil and gas mixture carrying the steam is led out of the retort through the gas collection umbrella.

(2) Retorting section

The dried oil shale exchanges heat with the hot recycle gas that passes through the section, as well as with the hot gas mixture flowing from the lower gasification section. Specifically, when the oil shale is heated to 330 °C, low-boiling-point volatile fractions start to form. In the temperature range of 350–550 °C, the oil shale releases a large amount of tar. The generated tar gases volatilize upward and are then led out through the gas collection umbrella.

(3) Gasification section

The gasification section is primarily located in the lower part of the retort, where reduction reactions and oxidation reactions mainly occur. In the reduction reaction, after semi-coke from the retorting section absorbs physical heat from hot gases generated in the oxidation reaction, some fixed carbon in the semi-coke reacts with water vapor to generate CO and H_2. The resulting water gas combines with gases from the gasification section to form a gas mixture that rises into the upper retorting section, while the semi-coke moves downward to undergo oxidation reactions.

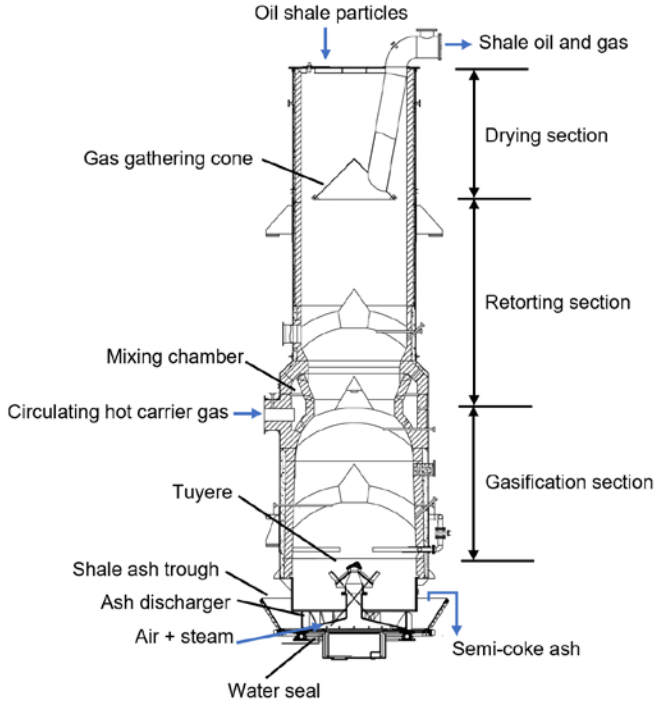

Fig. 1. Schematic structure of each section of the oil shale retort.

In the oxidation reaction, the fixed carbon in the shale semi-coke undergoes a vigorous oxidation reaction with the saturated air at 75–85 °C that is fed in, generating high-temperature products with a temperature greater than 700 °C, such as CO_2, CO, and shale ash. The newly formed gases mix with N_2 in the air to form a gas mixture. The gas mixture offers essential heat for the semi-coke reduction gasification reaction. At the same time, the shale ash produced by the reaction enters the cooling section.

2.2. Establishment of mathematical models

2.2.1. Modeling method

By discretizing the heat exchange field inside the retort, the energy balance equations for each section of the retort were established. These equations form a system of equations that can be solved discretely to effectively describe the characteristics of the high-temperature heat exchange field [12, 13].

Figure 2 shows the input and output parameters of the mathematical model. The accuracy and comprehensiveness of these parameters are crucial for the validity of the model. By properly selecting and adjusting these parameters, the complexity and dynamic changes within the heat exchange field in the retort can be captured more accurately [14]. The model's input parameters cover all aspects of the heat exchange field, whereas the output parameters provide key information about the simulation results.

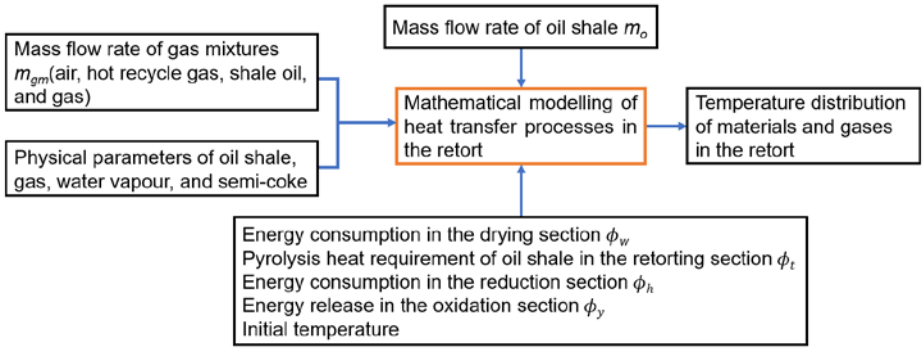

Fig. 2. Input and output parameters of mathematical models of heat transfer processes.

Table 1. Parameters specified in the modeling

Parameter	Value
Oil shale initial temperature	23 °C
Oil shale particle size	12~75 mm
Thermal conductivity of oil shale	1 W/(m·K) [15]
Apparent density of oil shale	1900 kg/m^3
Oil shale specific heat capacity	967 J kg^{-1} °C^{-1}
Oil shale moisture content	7.5%
Hot recycle gas density	1.22 kg/m^3
Shale ash specific heat	1088 J kg^{-1} °C^{-1}
Density of mixed gas	1.08 kg/m^3 [16]
Hot air density	1.293 kg/m^3
Loss factor of oil shale	0.069 [17]
Mean retort diameter	2750 mm
Mass flow rate of oil shale at inlet	1.375 kg/s
Mass flow rate of air at inlet	0.479 kg/s
Mass flow rate of hot recycle gas at inlet	0.289 kg/s

2.2.2. Assumptions

In view of the complex heat transfer process in the oil shale retorting, the following assumptions were made:

(1) It was assumed that the heat dissipation loss of the retort wall was negligible.

(2) It was assumed that the influence of radiation heat transfer in the retort was negligible.

(3) It was assumed that the material layer and gas properties were uniform within each section.

(4) The average particle size of oil shale particles in the actual retorting process was used instead of the actual particle size.

(5) The impact of heat transfer caused by the generation of oil and gas from the pyrolysis of organic matter during the oil shale retorting process was not considered.

2.3. Mathematical model

2.3.1. Theoretical basis of gas-solid convection heat transfer in oil shale retorts

During oil shale retorting, the solid material descends slowly and passes through the drying section. The hot recycle gas passes vertically through the material layer, exchanging heat with oil shale particles. This not only cools the semi-coke but also promotes the pyrolysis of the oil shale. The complex gas flow and heat transfer within the pores, owing to the small pore diameters and irregular shapes between the oil shale blocks, pose challenges for accurate mathematical simulation. Thus, the material layer was treated as a porous medium to account for heat transfer between the gas and solid phases.

The local non-thermal equilibrium double energy equation for convective heat transfer in porous media has been used to analyze the heat transfer process between gas and solid phases. Oil shale particles and gases were treated as distinct continuous media. Within the volume unit defined by the zones, the average temperatures of the gas and solid regions were determined and considered as the average temperatures of the gas phase and solid phase objects, respectively. These temperatures represent the thermal state within the same characteristic volume, and the heat transfer process within the porous medium is treated as a heat exchange between these two phases. The corresponding generalized system of equations is as follows:

$$\varepsilon\left(\rho c_p\right)_f \frac{\partial t_f}{\partial \tau} + \left(\rho c_p\right)_f v \cdot \nabla t_f = \nabla \cdot \left(\lambda_{feff} \nabla t_f\right) - h_{v,s-f}\left(t_f - t_s\right), \tag{1}$$

$$(1-\varepsilon)(\rho c_s)\frac{\partial t_s}{\partial \tau} = (1-\varepsilon)\nabla \cdot \left(\lambda_{seff} \nabla t_s\right) + h_{v,s-f}\left(t_f - t_s\right).^{1} \tag{2}$$

[1] For symbols used in the equations, please refer to the Nomenclature at the end of this article.

Equations (1) and (2) are the differential equations for gas-solid heat transfer. The heat transfer process within the retort can be simplified to a gas-solid heat transfer process within a porous medium, thereby avoiding the consideration of other complex heat transfer phenomena, such as solid-solid and gas-gas heat exchanges, during the analysis of discrete equations.

Given that adjacent oil shale blocks are in point contact and have a small thermal conductive area, and considering the small thermal conductivity of oil and gas in the gas stream, the thermal conductive fluxes between the material layers and between the gas stream and the material layers can be neglected in comparison to convective heat transfer. Therefore, the heat transfer between the gas and the material layer can be simplified to the expression shown below [16–20]:

$$\phi_{s-f} = h_{v,s-f}\left(t_s - t_f\right), \tag{3}$$

where the convective heat transfer coefficient $h_{v,s-f}$ per unit area between the material layer and gas can be determined by Achenbach's criterion relation [21, 22], as shown below:

$$h_{v,s-f} = \frac{6h_{sf}\left(1-\varepsilon\right)}{d_p}, \tag{4}$$

where h_{sf} is determined as follows:

$$Nu = \frac{h_{sf}d_p}{\lambda_f} = 2.0 + 0.6Pr^{1/3}Re^{1/2}. \tag{5}$$

In Equation (5), the values of *Pr* and *Re* can be obtained by solving the following equations:

$$Pr = \frac{\left(\mu c_p\right)_f}{\lambda_f}, \tag{6}$$

$$Re = \frac{\varepsilon\rho_r d_{\mathrm{p}} u}{\mu_{\mathrm{f}}}. \tag{7}$$

2.3.2. Mathematical modeling of oil shale retort

A discretization method was applied to solve the heat transfer process within the retort by dividing the entire heat transfer region into small sections. The temperature and physical parameters were assumed to be uniform within each section. By discretizing the heat-transfer region, an energy-balance equation can be established for each section. This series of equations forms a system, and by solving this system, it is possible to characterize the heat transfer between the gas and solid in a discrete manner. Figure 3 shows the heat-transfer process diagrams for these three sections.

The heat transfer equations for each section of the retort can be established based on the energy conservation equation and the heat transfer equation

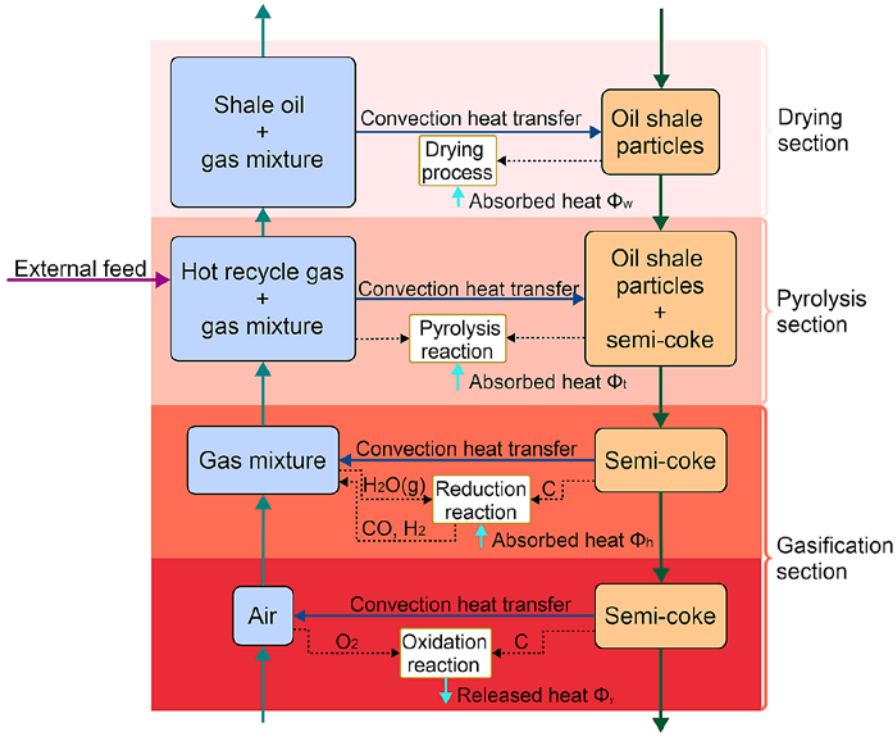

Fig. 3. Heat transfer process diagram for oil shale retort.

between gas and solid phases. It should be particularly noted that there is a unique source term in the energy conservation equation for each section. In the gasification section, the source term includes the chemical heat released by the combustion of semi-coke and the heat absorbed during the gasification of semi-coke; in the retorting section, the source term is the heat absorbed during the pyrolysis of oil shale; and in the drying section, the source term is the latent heat consumed by the evaporation of water. By accurately considering these source terms, the heat transfer process in each section of the retort can be more accurately described. The equations for each section are shown as Equations (8)–(11).

Gasification section:

(1) Oxidation reaction:

$$\begin{cases} \phi_{go-in} + \phi_{so-in} = \phi_{go-out} + \phi_{so-out} - \phi_y \\ \phi_{go-in} - \phi_{go-out} = m_{go,i-1} c_{go,i-1} t_{go,i-1} - m_{go,i} c_{go,i} t_{go,i} = -h_{o,i} V (t_{so,i} - t_{go,i}) - \phi_y \\ \phi_{so-in} - \phi_{so-out} = m_{so,i+1} c_{so,i+1} t_{so,i+1} - m_{so,i} c_{so,i} t_{so,i} = h_{o,i} V (t_{so,i} - t_{go,i}) \end{cases}, \quad (8)$$

(2) Reduction reaction:

$$\begin{cases} \phi_{gr-in} + \phi_{sr-in} = \phi_{gr-out} + \phi_{sr-out} + \phi_h \\ \phi_{gr-in} - \phi_{gr-out} = m_{gr,j-1} c_{gr,j-1} t_{gr,j-1} - m_{gr,j} c_{gr,j} t_{gr,j} = -h_{r,j} V (t_{sr,j} - t_{gr,j}) \\ \phi_{sr-in} - \phi_{sr-out} = m_{sr,j+1} c_{sr,j+1} t_{sr,j+1} - m_{sr,j} c_{sr,j} t_{sr,j} = h_{r,j} V (t_{sr,j} - t_{gr,j}) + \phi_h \end{cases} . \quad (9)$$

Retorting section:

$$\begin{cases} \phi_{gt-in} + \phi_{rws-in} + \phi_{st-in} = \phi_{gt-out} + \phi_{st-out} + \phi_t + \phi_{g-t} \\ \phi_{gt-in} + \phi_{rsw-in} - \phi_{gt-out} = m_{gt,k-1} c_{gt,k-1} t_{gt,k-1} - m_{gt,k} c_{gt,k} t_{gt,k} \\ = -h_{t,k} V (t_{st,k} - t_{gt,k}) + \phi_t + m_{t,k} c_{gt,k} (t_{gt,k} - t_{st,k}) \\ \phi_{st-in} - \phi_{st-out} = m_{st,k+1} c_{st,k+1} t_{st,k+1} - m_{st,k} c_{st,k} t_{st,k} = h_{t,k} V (t_{st,k} - t_{gt,k}) \end{cases} . \quad (10)$$

Drying section:

$$\begin{cases} \phi_{gd-in} + \phi_{sd-in} = \phi_{gd-out} + \phi_{sd-out} + \phi_w + \phi_{g-w} \\ \phi_{gd-in} - \phi_{gd-out} = m_{gd,m-1} c_{gd,m-1} t_{gd,m-1} - m_{gd,m} c_{gd,m} t_{gd,m} = -h_{d,m} A (t_{sd,m} - t_{gd,m}) \\ + m_w c_{w,m} (t_{gd,m} - t_{am}) \\ \phi_{sd-in} - \phi_{sd-out} = m_{sd,m+1} c_{sd,m+1} t_{sd,m+1} - m_{sd,m} c_{sd,m} t_{sd,m} = h_{d,m} V (t_{sd,m} - t_{gd,m}) + \phi_w \end{cases} . \quad (11)$$

2.3.3. Solution and validation of the model

(1) Solution of the model

Separately, the equations for the above four sections were linked to form a set of energy-balance equations for each model section. The solution model for the temperature field in each of these processes can be expressed in the form of a matrix equation:

$$[A]\vec{t} + \vec{C} = 0 . \quad (12)$$

To facilitate the model, the height of each model section was divided into 0.01 m. Assuming that there are N model sections in the retort, N_1 model sections are required for the gasification process of semi-coke, N_2 model sections for the retorting process of shale semi-coke; and N_3 model sections for the drying process of shale semi-coke, that is, $N = N_1 + N_2 + N_3$. The following gasification section was used as an example to establish a system of matrix equations to solve the problem, and the remaining three sections were listed in the same way.

(a) Matrix solver:

$$\vec{t}_1 = \left(t_{s,1}, t_{g,1}, \cdots, t_{s,i}, t_{g,i}, \cdots, t_{s,N_1}, t_{g,N_1} \right)^T . \quad (13)$$

Vector $\vec{t}_1$ has $2N_1$ elements.

Matrix $[A]_1$ is as follows:

$$[A]_1=\begin{pmatrix} h_{s-g}V & \psi_1 & 0 & 0 & 0 & \cdots & 0 & \cdots & 0 & 0 \\ \xi_1 & h_{s-g}V & m_{so,1}c_{so,1} & 0 & 0 & 0 & \ddots & 0 & 0 & 0 \\ 0 & m_{go,2}c_{go,2} & h_{s-g}V & \psi_2 & 0 & 0 & 0 & \ddots & 0 & 0 \\ 0 & 0 & \xi_2 & h_{s-g}V & m_{so,2}c_{so,2} & 0 & 0 & 0 & \ddots & 0 \\ 0 & 0 & 0 & \ddots & \ddots & \ddots & 0 & 0 & 0 & \vdots \\ 0 & 0 & 0 & 0 & m_{go,i}c_{go,i} & h_{s-g}V & \psi_i & 0 & 0 & 0 \\ \vdots & \ddots & 0 & 0 & 0 & \xi_i & h_{s-g}V & m_{so,i}c_{so,i} & 0 & 0 \\ 0 & 0 & \ddots & 0 & 0 & 0 & \ddots & \ddots & \ddots & 0 \\ 0 & 0 & 0 & \ddots & 0 & 0 & 0 & m_{go,N_1}c_{go,N_1} & h_{s-g}V & \psi_{N_1} \\ 0 & 0 & \cdots & 0 & \cdots & 0 & 0 & 0 & \xi_{N_1} & h_{s-g}V \end{pmatrix}. \quad (14)$$

Included among these:

$$\xi_i=-(m_{so,i}c_{so,i}+h_{o,i}V), \quad (15)$$

$$\psi_i=-(m_{go,i}c_{go,i}+h_{o,i}V). \quad (16)$$

Vector $\vec{C}$ is as follows:

$$\vec{C}=\begin{pmatrix} m_{go,0}c_{go,0}t_{go,0}+\phi_y \\ 0 \\ \vdots \\ \phi_y \\ 0 \\ \vdots \\ \phi_y \\ m_{so,N_1}c_{so,N_1}t_{so,N_1} \end{pmatrix}. \quad (17)$$

(b) Physicochemical reaction parameters in the model:

The temperature at which the pyrolysis of oil shale is initiated increases with the extent of retorting. The onset of pyrolysis for oil shale particles occurs at 180 °C. Consequently, it is assumed that the water within the oil shale particles evaporates linearly between 25 and 180 °C, and the volatile fraction precipitates linearly between 180 and 550 °C [23, 24]. The special heat release of each section in the oil shale retort is shown in Table 2.

Table 2. Heat composition of each section in the retort

Pyrolytic heat release characteristics of materials in the retort	Symbol	Calorific value
Heat released by unit mass of solid combustion in the oxidation reaction	q_o	32791670 J/kg
Heat absorbed by unit mass of solid in the redox reaction (water-gas reaction)	q_r	7508300 J/kg
Heat required for releasing volatiles via pyrolysis of unit mass of solid in the retorting section	q_t	235559 J/kg [25]
Latent heat of water evaporation and gasification in the drying section	q_d	2442000 J/kg [26]

Gasification section

Oxidation reaction:

$$\begin{cases} m_y = \dfrac{m_{y,all}}{N_1} \\ \phi_y = q_o \times m_y \\ m_{go,i} = m_{go,0} + (i-1) \times m_y \\ m_{so,i} = m_{so,0} + i \times m_y \end{cases}. \tag{18}$$

Reduction reaction:

$$\begin{cases} m_h = \dfrac{m_{h,all}}{N_2} \\ \phi_h = q_r \times m_h \\ m_{\mathrm{gr},j} = m_{go,N_1} + (j-1) \times m_h \\ m_{sr,j} = m_{so,N_1} + j \times m_h \end{cases}. \tag{19}$$

Retorting section:

$$\begin{cases} m_t = \dfrac{m_{t,all}}{N_3} \\ \phi_t = q_t \times m_t \\ m_{gt,k} = m_{gr,N_2} + (k-1) \times m_t \\ m_{st,k} = m_{sr,N_2} + k \times m_t + m_{chc} \end{cases}. \tag{20}$$

Drying section:

$$\begin{cases} m_w = \dfrac{m_{w,all}}{N_4} \\ \phi_w = q_d \times m_w \\ m_{gd,m} = m_{gt,N_3} + (m-1) \times m_w \\ m_{sd,m} = m_{st,N_3} + m \times m_w \end{cases} . \quad (21)$$

(2) Validation of the model

To validate the accuracy of the mathematical simulation method, this study compared and analyzed the numerical simulation results of the gas-phase temperature distribution within the retort against real-time monitoring data of gas phase temperature distribution obtained during actual industrial production processes. The specific measurement locations and comparative results are shown in Figures 8 and 4, respectively. The comparative analysis results indicate that the maximum relative deviation between the measured gas-phase temperature data and the simulation results is within 8%. Although a certain margin of error exists, considering the simplified assumptions of the model and the requirements of practical engineering applications, this level of deviation is deemed reasonably acceptable. These findings validate the reliability of the computational model in reflecting the actual thermodynamic characteristics under operating conditions.

3. Results and discussion

3.1. Gas-solid temperature distributions

Figure 5 depicts the temperature distributions of the oil shale particles and mixed gas, as well as the temperature differences between them, within the chamber of a gas retort. The retorting process was conducted at 520 °C, with oil shale particles having a porosity of 0.5.

Within the retort, the gas-solid phase exhibits typical counter-current heat transfer characteristics along the retort height direction.

At ambient temperature, the oil shale is fed from the retort top and gradually descends under gravity. Oil shale is progressively heated via thermal exchange through intensive contact with the upward-flowing hot gas carrier. Oil shale undergoes sequential drying and retorting processes, yielding oil vapors and semi-coke. During this process, the gas phase is cooled and the oil vapors become gaseous components. Concurrently, the hot recycle gas is introduced into the retorting section, transferring its thermal energy to the oil shale. This causes a certain degree of temperature elevation in the gas phase. Finally, the gas phase exits the retort at approximately 120 °C.

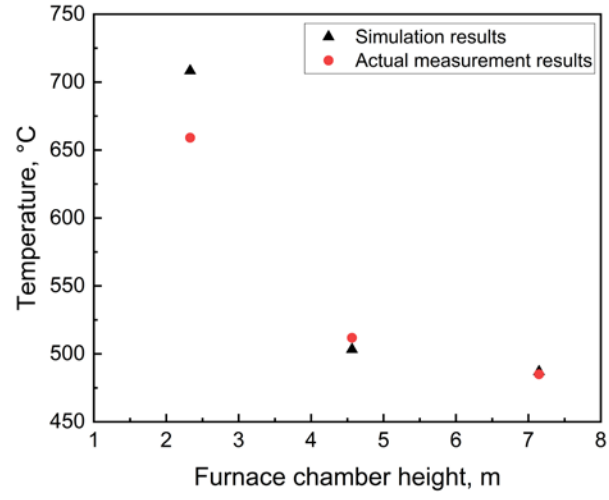

Fig. 4. Comparison of simulation and experiment.

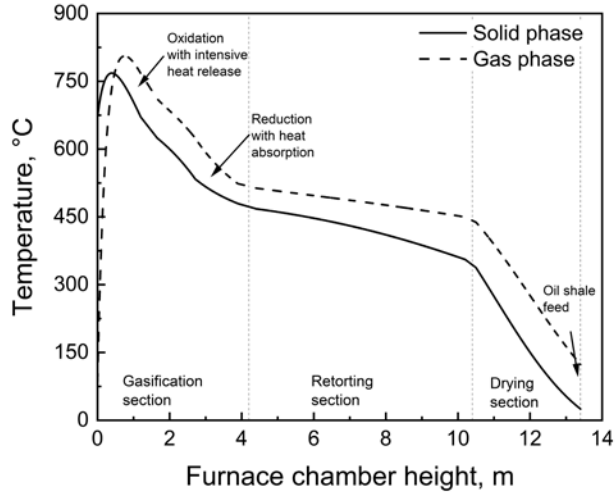

Fig. 5. Gas-solid temperature distribution.

The semi-coke moves downward into the gasification section, where it fully contacts and absorbs heat from the gas phase, undergoing the water-gas shift reaction. This effectively prevents excessive temperature elevation of the semi-coke, maintaining it stably between 500–550 °C. During this process, the gas phase is cooled, and the gaseous products generated from the water-gas shift reaction also join the gas phase.

The semi-coke unreacted in the reduction reaction continues to move downward, mixes with air supplied from the bottom, and undergoes oxidative

combustion. During this process, the semi-coke reacts completely with oxygen, releasing substantial heat that causes its temperature to rise rapidly to approximately 750 °C. Simultaneously, the high-temperature combustion products enter the gas phase, elevating the gas temperature significantly to around 850 °C. During combustion, the semi-coke is converted into high-temperature semi-coke ash, which exchanges heat with the cold air introduced from the bottom of the retort. The heat from the semi-coke ash is transferred to the cold air, causing a decrease in its temperature, while the temperature of the gas phase is further increased. Ultimately, the semi-coke ash is cooled to around 65 °C, and then discharged from the retort.

Changes in parameters such as hot air volume, hot recycle gas temperature, and porosity affect the heat transfer process and heat transfer intensity inside the retort. Specifically, the variation in porosity (as shown in Eq. (5)) influences the gas-solid heat transfer coefficient. Meanwhile, the hot air volume and hot recycle gas temperature alter the thermophysical properties of the mixed gas in the retort and the gas mass involved in reactions at different stages. These changes further affect the heating degree of oil shale particles, leading to variations in both the location where oil shale undergoes retorting and the time required for complete retorting. Under different parameter conditions, the reasonable retort height is defined as the height at which oil shale just finishes pyrolysis inside the retort. This height ensures no redundant space while avoiding impacts on product yield and quality.

The curve distribution of the retort temperature varying with height in Figure 5 indicates that, to achieve the retorting of oil shale, the actual length of each section of the retort body derived from production data is as follows: the gasification section is 4.2 m high, the retorting section is 6.2 m high, and the drying section is 3.0 m high, with the total height of the retort being 13.4 m. For the current Fushun-type retort in the plant, the internal reaction height (excluding the ashtray and air distributor head) measures 12.6 m. The relative error between this measured height and the mathematically simulated height is 6.3%. Although this error exists, it falls within an acceptable range, which also verifies the feasibility of the mathematical simulation.

3.2. Analysis of the effect of thermodynamic parameters on the retorting process

3.2.1. Orthogonal experimental design data and orthogonal table

In this study, an orthogonal experiment was carried out. Its purpose was to analyze how hot air volume, hot recycle gas temperature, and oil shale interparticle porosity affect the thermal efficiency of the retort. The retort height needed to distill the same quality of oil shale served as an indicator of the retort's thermal efficiency. Specifically, a lower required retort height indicated a higher thermal efficiency of the retort. An orthogonal experiment

is a multifactorial experimental research method in which a few representative experimental points can be selected from a large number of experimental combinations. This experimental design enables a substantial reduction in the number of experiments while ensuring the validity of scientific analysis. Range and variance analyses are commonly used to analyze the results of orthogonal experiments. The polar deviation method is simple, fast, and requires minimal calculation, but it also has shortcomings, mainly because it does not separately analyze random or conditional errors; however, the variance method can address this deficiency [27]. In this study, we employed the variance method for data processing and analysis. The detailed calculation method of variance analysis is referenced in [28, 29].

The orthogonal factor-level table used is presented in Table 3. Since the interaction of the factors was not considered, the $L_9(3^4)$ table was selected as the orthogonal table. Nine sets of simulations were required, according to the orthogonal experimental schedule, and each set of simulations was completed sequentially. Table 4 presents the orthogonal table used to study the multifactor effect levels. During the parameter selection process, the experimental parameters were determined based on the actual plant process and theoretical calculations. This was done to ensure several conditions. First, the hot air volume did not exceed 1.24 kg/s. Second, the hot recycle gas temperature was

Table 3. Orthogonal experimental factor level table

Level	Factors		
	Hot air volume, kg/s	Hot recycle gas temperature, °C	Porosity
	A	B	C
1	0.3996	516.07	0.4
2	0.4627	536.07	0.5
3	0.5258	556.07	0.6

Table 4. Orthogonal experimental design and results

Case	Factors				Retort height, m
	A	B	C	Error	
1	1	1	1	1	16.21
2	1	2	2	2	15.15
3	1	3	3	3	14.58
4	2	1	2	3	14.22

Continued on the next page

Table 4. *Continued*

Case	Factors				Retort height, m
	A	B	C	Error	
5	2	2	3	1	13.81
6	2	3	1	2	12.50
7	3	1	3	2	13.24
8	3	2	1	3	12.07
9	3	3	2	1	11.75

close to 550 °C. Additionally, the porosity was optimized using the nonlinear value-taking method in order to identify the optimal parameter combination.

3.2.3. Analysis of orthogonal experiment results

Nine cases were designed in the orthogonal experiment, and the variation diagrams of gas-solid temperature with retort height distribution for each case were analyzed. The distribution law of the maximum retort height is consistent with that in the orthogonal experiment table. The specific variation law of gas-solid temperature distribution with height under each working condition is shown in Figure 6.

It can be observed that regarding the variation of temperature distribution with retort height from Case 1 to Case 9, the overall variation law shows consistency. Among these cases, Case 1 exhibits the highest retort height, which is 16.21 m, while Case 9 is the working condition with the lowest retort height, at 11.75 m. Based on the analysis of retort heights at different levels, the retort height varies with the change of working conditions.

In the lower region of the retort, the gas and solid phase temperatures of all cases rise rapidly to relatively high levels, with peak values approaching or exceeding 750 °C; this is due to the large amount of heat released by the intense combustion reactions occurring in this region. In contrast, in the drying section of the upper retort, the gas and solid phase temperatures decrease continuously and eventually reach relatively low levels. This is because the newly added oil shale particles need to absorb heat from the mixed gas in the retort, resulting in a rapid temperature drop of both phases in this region.

As the retort height increases, the temperatures of the two phases show an overall decreasing trend, but there are significant differences among different cases: the temperature drop in Cases 1–3 is relatively gentle, and the gas phase temperature is consistently higher than the solid phase temperature, with a stable temperature difference between them. This is because the high-temperature gas generated by combustion is used to heat the solid phase,

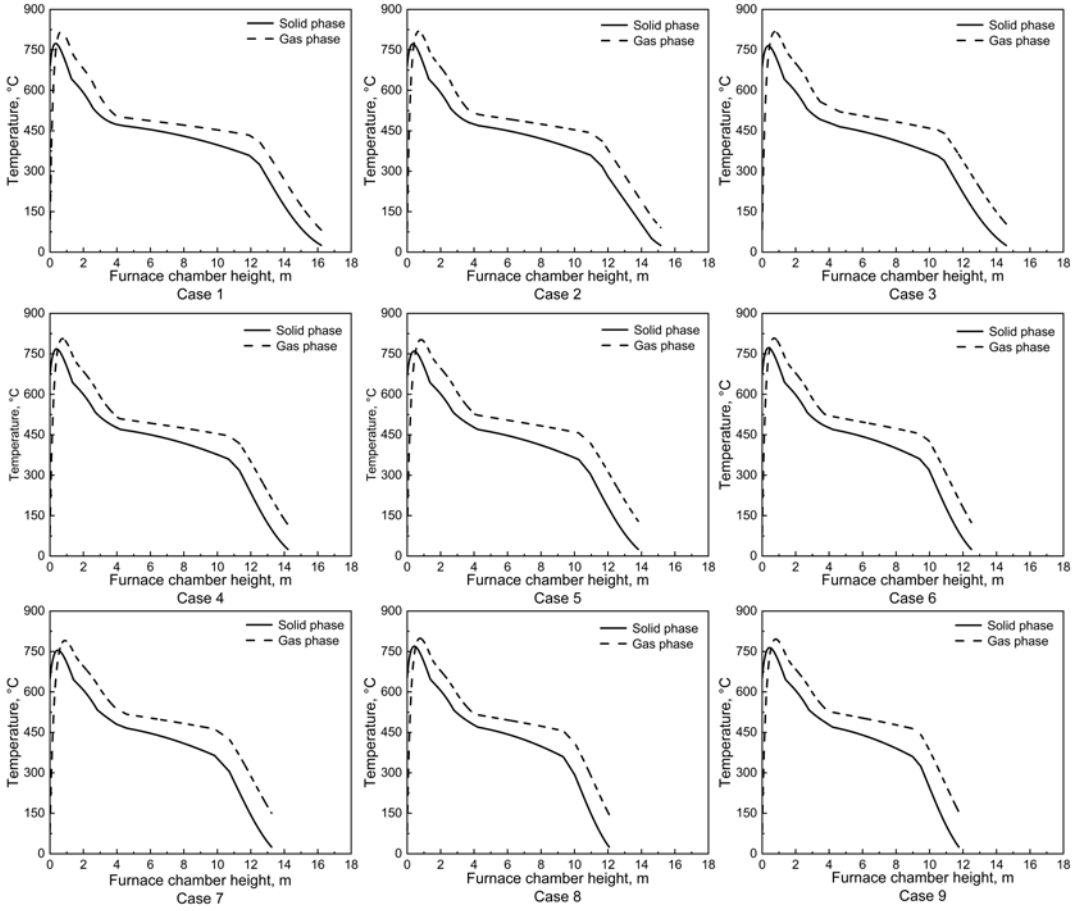

Fig. 6. Gas-solid temperature distribution diagrams for Cases 1–9.

leading to the gas phase temperature remaining continuously higher than the solid phase temperature. The magnitude of the solid phase temperature drop in Cases 4–6 is significantly greater than that in Cases 1–3. The main reason is that the increased hot air volume enhances the heat transfer process with the solid phase, resulting in a larger decrease in the solid phase temperature. The temperature decreasing trend in Cases 7–9 is consistent with the previous cases, but there are differences in specific values and decreasing rates. Along the retort height direction, the temperatures of the gas and solid phases drop more rapidly – especially at the position corresponding to the retorting section, where the length of this section is significantly shortened. This is because, as the hot air volume further increases, the heat supply from the generated gas in the gasification section is enhanced, which facilitates the progress of the retorting reaction.

In general, all cases follow the overall trend of rapid temperature rise to a peak in the lower part of the retort, gradual temperature drop in the middle part, and continuous temperature drop to a relatively low value in the upper part. However, differences exist among cases in terms of temperature change rate, temperature difference between solid and gas phases, and other parameters. These differences are related to factors such as the amount of hot air fed into the retort, the temperature of hot recycle gas, and porosity, which reflect the distribution characteristics of the temperature field in the retort under different working conditions. The height of the retort is affected by changes in different parameters. For example, in Cases 1–9: when the hot recycle gas temperature was consistently 516.07 °C (Cases 1, 4, 7), the retort height decreased from 16.21 m to 13.24 m as the hot air volume increased from 0.3996 kg/s to 0.5258 kg/s; when the hot recycle gas temperature was consistently 536.07 °C (Cases 2, 5, 8), the retort height decreased from 15.15 m to 12.07 m with the increase in the hot air volume; and when the hot recycle gas temperature was consistently 556.07 °C (Cases 3, 6, 9), the retort height decreased from 14.58 m to 11.75 m, following the same trend of hot air flow rate increase. This phenomenon can be attributed to the enhanced heat transfer efficiency inside the retort caused by the increased hot air volume, which promotes the heating of oil shale particles and accelerates the retorting process, thereby leading to a reduction in retort height.

Simulation studies were conducted to analyze how three factors (hot air volume, hot recycle gas temperature, and oil shale interparticle porosity) influence the chamber height of the retort. This analysis aims to rank the factors according to their influence magnitude and uncover the intrinsic relationship between each factor and the key performance indicators of the retorting process. This study employed two statistical methods, range analysis and variance analysis, to investigate the effects of different experimental factors on retort height. Range analysis offers a straightforward way to understand the influence range of each factor, while variance analysis provides a more comprehensive evaluation by considering the variability within the data.

In this study, the orthogonal experimental method was employed to systematically investigate the effects of factors A, B, and C on the retort height standard. The results of range analysis showed that the primary and secondary order of the effects of the three factors on the index was A > B > C, with their range (R) values being 2.96, 1.61, and 0.28, respectively. Analysis of variance further confirmed that both factor A ($F = 75.822$, $P = 0.013$) and factor B ($F = 22.233$, $P = 0.043$) had significant effects on the retort height standard, while the effect of factor C ($F = 0.693$, $P = 0.591$) did not reach the statistical significance level.

The results indicated that factor A was the most critical parameter for controlling the retort height standard, factor B played an auxiliary regulatory role, and factor C had no significant effect on the results within the level range set in the experiment. Taking the reduction of retort height as the optimization

Table 5. Influence of each factor on the mean retort height

Analytical method	Item	Factor			Error
		A	B	C	
Range analysis	K_1	15.31	14.56	13.59	13.92
	K_2	13.51	13.68	13.71	13.63
	K_3	12.35	12.94	13.88	13.62
	R	2.96	1.61	0.28	0.30
Variance analysis	Sum of squares of deviations	13.351	3.915	0.122	0.176
	Freedom	2	2	2	2
	F ratio	75.822	22.233	0.693	
	P	0.013*	0.043*	0.591	
	Significance	*	*	-	

objective, the recommended optimal combination of process parameters was A3 and B3, and the level of factor C could be selected according to actual production conditions. Combining the findings from analytical methods, hot air volume was identified as the key factor affecting the effectiveness of oil shale retorting production [30]. Meanwhile, the effects of hot recycle gas temperature and porosity should not be overlooked.

The mean values of each factor in the orthogonal experiment were plotted for comparative analysis. Figure 7 presents the mean value comparison diagram of the orthogonal experiment, from which it can be observed that factor A (hot air volume), factor B (hot recycle gas), and factor C (porosity) all exert influences on the experimental index. With the increase of factor A (hot air volume), the variation trends of the index under different hot recycle gas temperatures exhibit significant differences: under condition B1, the retort height decreases continuously, from 16.21 to 13.24 m; under condition B2, it remains relatively stable, fluctuating between 15.15 and 12.07 m; under condition B3, it shows fluctuation, yet the overall height also decreases, dropping to a minimum of 11.75 m.

Comprehensive analysis indicates that, to improve the thermal efficiency of the retorting retort, a higher hot air volume should be combined with the hot recycle gas temperature at level B3. This combination can reduce the retort height to 11.75 m, which is the lowest value among all combinations. Meanwhile, the distribution of the three level points of porosity shows that its influence is relatively weak. The results of the orthogonal experiment reveal that hot air volume is the key factor affecting the retort height. Furthermore, range analysis and analysis of variance confirm that the regulation of hot

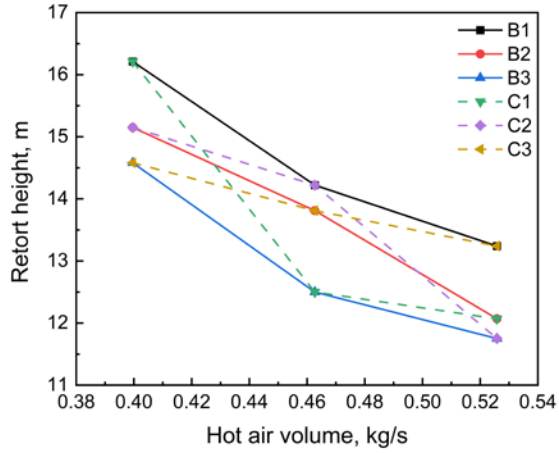

Fig. 7. Mean value comparison diagram of factor A with factors B and C.

air volume is significantly positively correlated with the retorting thermal efficiency – specifically, an increase in the hot air volume can significantly enhance the retorting thermal efficiency.

4. Study on simulation and optimization of hot air parameters for the Fushun-type retort

Based on the above orthogonal experiment results, it is known that the factor with the greatest influence on the height of the retorting retort is the hot air volume. This is a key parameter for regulating the heat supply. An increase in the hot air volume can enhance the kinetic process of the fixed carbon combustion reaction in the gasification section, promote its full combustion, and release more heat, thereby providing sufficient heat support for retorting. Meanwhile, the increase in fixed carbon combustion heat can optimize the distribution of the temperature field in the retort and affect the height of the material layer, the range of the pyrolysis zone, and other factors. To improve the accuracy of simulation results and conduct diversified research, computational fluid dynamics (CFD) software was used to perform simulations on the optimal working condition of the orthogonal experiment.

The water and oxygen in the hot air undergo redox reactions with the fixed carbon (C) in the semi-coke. These reactions mainly occur in the gasification section. The hot air volume has the strongest influence on the gasification section of the retorting retort; therefore, modeling was conducted for the gasification section. All structures used in the simulation adopt the actual parameters of the factory. Model establishment and mesh division were carried out for the gasification section of the retorting retort. The specific modeling area can be seen in Figure 8.

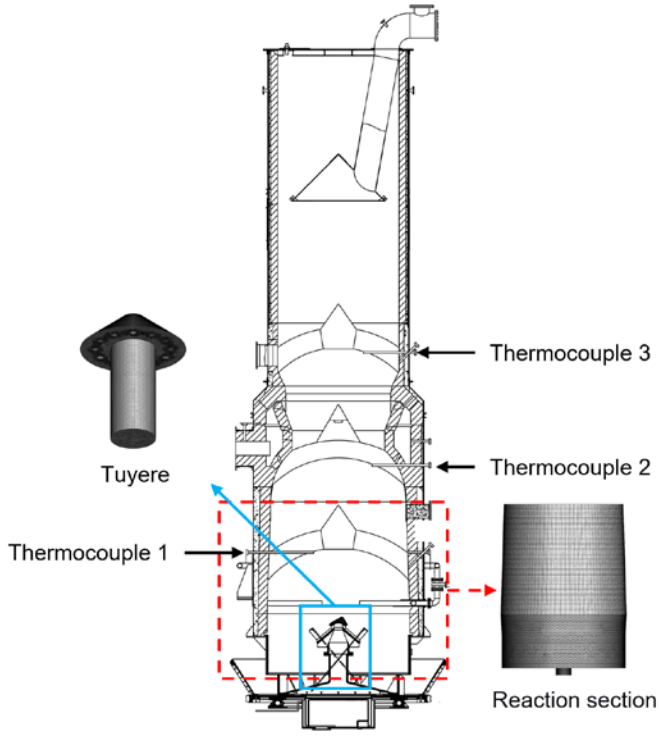

Fig. 8. Schematic diagram of model establishment and mesh division.

Based on the thermocouple position specified in Figure 8, a comparison was conducted between the simulation results and the temperature measurements obtained from the corresponding thermocouples in factory tests. It was found that the error between the CFD simulation data and the measured data is within 5%, which is within a reasonable and acceptable range. This effectively confirms the accuracy of the simulation results.

Figure 9 shows the temperature distribution contour maps of the reaction section under different working conditions. In the gasification section of the retorting retort, heat is mainly derived from the intense oxidation reaction of fixed carbon in semi-coke. In Figure 9(a), the high-temperature zone is mainly distributed in the lower part of the gasification section. Driven by gravity, the fixed carbon (C) in semi-coke falls to the lower part of the gasification section and undergoes an oxidative combustion reaction with oxygen in the introduced hot air, releasing heat. In contrast, in Figure 9(b), the red high-temperature zone is concentrated in the lower-middle part, with the high-temperature zone located relatively higher. This is because the velocity at the hot air inlet is relatively high, resulting in a slow falling speed of semi-coke, and the oxidative combustion reaction occurs in the relatively higher region.

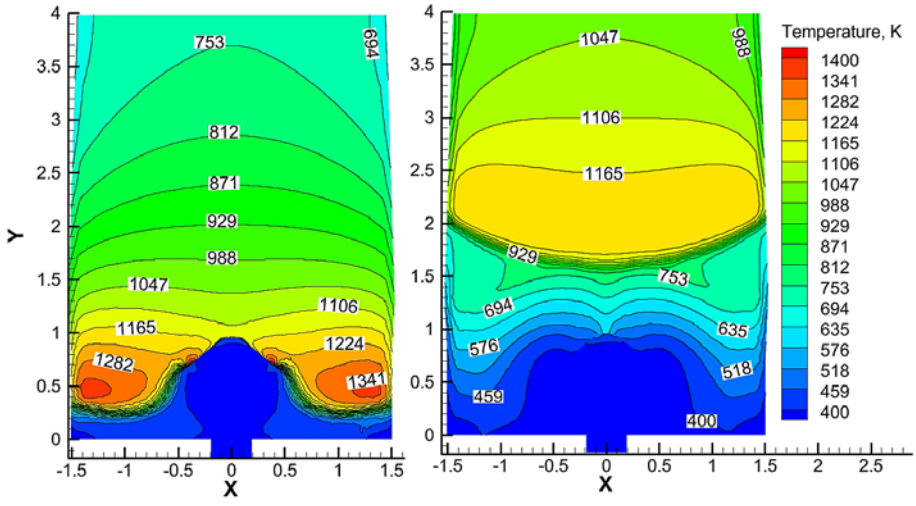

(a) 0.4667 kg/s (b) 0.5258 kg/s

Fig. 9. Temperature distribution contour maps in the gasification section: current factory data with a hot air volume of 0.4667 kg/s (a); the optimal hot air volume of 0.5258 kg/s selected by the orthogonal experiment (b).

The heat released by combustion in the gasification section moves upward along with the high-temperature flue gas, forming an obvious temperature gradient, which presents a gradual temperature decrease from bottom to top. The lower part of the gasification section is a low-temperature zone, mainly because this region is the location of the hot air inlet, where the air velocity is relatively high, driving the airflow upward and preventing the occurrence of combustion reactions in the lower part.

It can be seen in Figure 9 that there are significant differences in the distribution of high-temperature zones under different hot air volumes. This is mainly because increasing the hot air volume leads to an increase in the inlet velocity, which affects the heat transfer behavior and the movement behavior of semi-coke particles in the retort, resulting in the upward shift of the high-temperature zone.

According to the literature, the heat sources required for oil shale retorting are divided into three parts: (1) 47% of the heat is provided by the self-generated gas in the gasification section; (2) 30% of the heat is provided by the hot recycle gas; and (3) 23% of the heat is provided by the heat exchange between the primary air and steam [31]. These three gas streams jointly form a heat carrier, which directly conducts heat exchange with oil shale. By analyzing the above two working conditions, the heat condition at the gas outlet of the gasification section was investigated to explore the contribution degree of the change in the hot air volume in the gasification section to the heat required for the pyrolysis of the oil shale gasification section.

According to the literature, the heat required for retorting 1 kg of oil shale is 989.951 kJ/kg [31]. Based on the CFD simulation results, the contribution of the two working conditions to oil shale retorting was analyzed. The results show that the self-generated gas heating proportion of the orthogonal working condition (59.288%) is higher than that of the current factory working condition (46.554%), as shown in Table 6. These data verify the feasibility of the orthogonal working condition and prove that it has more advantages in improving thermal energy utilization efficiency.

However, analysis based on the position of the temperature distribution contour maps shows that the high-temperature zone under the orthogonal experiment working condition is relatively higher, while under the current factory working condition, the high-temperature zone is mainly distributed in the lower part of the gasification section. A higher-positioned high-temperature zone may lead to a relatively high temperature in the retorting section, potentially causing over-retorting. To stabilize the high-temperature zone at a relatively lower position in the gasification section, reducing the air velocity at the hot air inlet is conducive to maintaining a stable high-temperature zone.

Table 6. Comparison of heat supply quantities

Parameter	Factory working condition	Orthogonal working condition
Mass flow rate at the inlet of the gasification section	0.272 kg/s	0.526 kg/s
Heat flux carried by generated gas per second	460.861 kJ	586.923 kJ
Heat supply proportion of generated gas	46.554%	59.288%
Heat required for retorting 1 kg of oil shale	989.95 1kJ	

Based on an in-depth investigation of thermal parameters, this study establishes that increasing the hot air volume is the most critical pathway for optimizing the retorting process, with its core mechanism being the intensification of the oxidation and exothermic process of fixed carbon in semi-coke. This finding illuminates the path for process innovation: the implementation of oxygen-enriched retorting technology by actively regulating the chemical composition of the inlet gas. By elevating the oxygen concentration in the inlet stream while maintaining an appropriate gas volume, the combustion reaction can be intensified more directly and efficiently, thereby significantly enhancing the self-sustaining heating capacity of the retort. Simulation results indicate that this technology has the potential to increase the heat supply proportion of the process-generated gas beyond 59.288%,

substantially reducing dependence on external heat sources such as circulating carrier gas, and thereby opening a highly promising technological route for energy conservation, consumption reduction, and efficiency enhancement in oil shale retorting processes.

To advance oxygen-enriched retorting technology from concept to industrial practice, future research should concentrate on several key directions. The foremost priority is to systematically explore the effects of different oxygen concentrations (e.g., 25–35%) on retorting thermal equilibrium, product yield, and overall energy consumption, to identify the optimal operational window for oxygen enrichment. Concurrently, it is essential to elucidate the oxidation reaction kinetics of semi-coke under oxygen-enriched conditions and its impact on heat transfer and product formation mechanisms in the upper retorting zones, thereby providing a theoretical foundation for process control. Finally, concerted efforts must be directed toward the system integration and engineering development of this technology, including the creation of coupling schemes with low-energy oxygen production processes, investigation of precise temperature field control strategies in the reaction zone under oxygen-enriched conditions, and comprehensive techno-economic and environmental benefit assessments, ultimately ensuring the safe, stable, and economical operation of this innovative process.

5. Conclusions

Mathematical models for the drying, retorting, reduction, and oxidation sections of the oil shale retort have been developed, yielding a set of energy balance equations for each section. Three typical parameters – hot air volume, circulating hot recycle gas temperature, and oil shale interparticle porosity – were analyzed through single-factor and multi-factor analyses. The aim was to determine the factors most influencing the height of the oil shale retort and to identify the optimal working conditions. Meanwhile, to improve accuracy, CFD simulation technology was used to conduct simulation and comparison between the factory working condition and the optimal working condition selected by the orthogonal experiment.

1. A numerical heat transfer model for each section of the Fushun-type retort has been established and its reliability verified. Subsequently, each section of the retort was optimized using this model. When the retort temperature is 520 °C, the recommended retort height is 13.4 m, with the gasification, retorting, and drying sections being 4.2 m, 6.2 m, and 3.0 m in height, respectively.
2. Orthogonal experimental analysis reveals that the factors influencing retort height, in descending order of significance, are hot air volume, hot recycle gas temperature, and porosity. Hot air volume plays a crucial role in the retorting process.

3. Based on the key finding that increasing the hot air volume optimizes the retorting process by intensifying the oxidation of fixed carbon, this study proposes an innovative strategy of oxygen-enriched retorting. By elevating the oxygen concentration in the inlet gas, this approach is expected to significantly enhance the system's self-sustaining heating capacity, thereby reducing reliance on external heat sources. Subsequent research should focus on determining the optimal oxygen concentration range, elucidating the associated reaction kinetics, and developing the necessary integrated engineering systems to promote the safe and efficient industrial application of this advanced retorting technology.

Data availability statement

All data, models, and code generated or used during this study are included in the article.

Acknowledgments

This study was financially supported by the Scientific Research Project of the Education Department of Liaoning Province (project No. L2020028) and Liaoning Provincial Department of Education unveils local projects (No. JYTMS20231421). We thank the reviewers for their careful reading of the manuscript and for providing valuable guidance and suggestions. The publication costs of this article were partially covered by the Estonian Academy of Sciences.

References

1. Yin, X. H., Cao, Z. B., Cao, C. Y., Lü, N. Simulation and optimization in shale oil condensation recovery system. *Journal of Petrochemical Universities*, 2019, **32**(3), 20–27. https://doi.org/10.3969/j.issn.1006-396X.2019.03.004
2. Wang, Q., Liu, J., Bai, J. R., Kong, L. W. Analysis on properties of shale oil pyrolyzed from oil shale at different heating rates. *Journal of Northeast Electric Power University*, 2011, **31**(1), 24–28.
3. Wang, Q., Xu, C. X., Chi, M. S., Zhang, H. X., Cui, D., Bai, J. R. FT-IR study on composition of oil shale kerogen and its pyrolysis oil generation characteristics. *Journal of Fuel Chemistry and Technology*, 2015, **43**(10), 1158–1166.
4. Nazzal, M. J. Influence of heating rate on the pyrolysis of Jordan oil shale. *Journal of Analytical and Applied Pyrolysis*, 2002, **62**(2), 225–238. https://doi.org/10.1016/S0165-2370(01)00119-X
5. Geng, Y. D., Liang, W. G., Liu, J., Cao, M. T., Kang, Z. Q. Evolution of pore

and fracture structure of oil shale under high temperature and high pressure. *Energy & Fuels*, 2017, **31**(10), 10404–10413. https://doi.org/10.1021/acs.energyfuels.7b01071

6. Pan, C. C., Liang, Q. F., Guo, X. L., Dai, Z. H., Liu, H. F., Gong, X. Characteristics of different sized slag particles from entrained-flow coal gasification. *Energy & Fuels*, 2016, **30**(2), 1487–1495.
7. Xu, L. F., Ma, Z. L., Zheng, L. J., Bao, F. Change of physical properties at different heating rates, time and water content for oil shale. *Petroleum Geology & Experiment*, 2018, **40**(4), 545–550. https://doi.org/10.11781/sysydz201804545
8. Han, X. X., Jiang, X. M., Cui, Z. G. Study of the combustion mechanism of oil shale semicoke in a thermogravimetric analyzer. *Journal of Thermal Analysis and Calorimetry*, 2018, **92**(2), 595–600. https://doi.org/10.1007/s10973-007-8659-6
9. Khalil, A. Oil shale pyrolysis and effect of particle size on the composition of shale oil. *Oil Shale*, 2013, **30**(2), 136–146. https://doi.org/10.3176/oil.2013.2.04
10. Tang, Y. B. A laboratorial study of spontaneous combustion characteristics of the oil shale in Fushun, China. *Combustion Science and Technology*, 2016, **188**(6), 997–1010. https://doi.org/10.1080/00102202.2015.1136301
11. Lu, H., Pan, H. D., Guo, C., Liu, X. Y., Wang, C. H., Yue, Y. Comparative study on pyrolysis kinetic model of Fushun oil shale. *Journal of Liaoning Petrochemical University*, 2020, **40**(1), 20–25. https://doi.org/10.3969/j.issn.1672-6952.2020.01.004
12. Luo, W. X., Yu, C. J., Wang, Q., Zhao, A., Ke, Y. L. Spatially discretised compensation method for coordinate transformation in large-scale metrology under nonuniform temperature field. *Measurement Science and Technology*, 2023, **34**(3), 035003. https://doi.org/10.1088/1361-6501/ACA2D0
13. Baruah, B., Tiwari, P. Effect of high pressure on nonisothermal pyrolysis kinetics of oil shale and product yield. *Energy & Fuels*, 2020, **34**(12), 15855–15869. https://doi.org/10.1021/ACS.ENERGYFUELS.0C02538
14. Rossiello, G., Uzair, M. A., Ahmadpanah, S. B., Rogora, M., Saponaro, A., Torresi, M. Integrated use of CFD and field data for accurate thermal analyses of oil/gas boilers. *Fuel*, 2023, **335**, 126931. https://doi.org/10.1016/j.fuel.2022.126931
15. Zhu, J., Yi, L., Yang, Z., Li, X. Numerical simulation on the in situ upgrading of oil shale reservoir under microwave heating. *Fuel*, 2021, **287**, 119553. https://doi.org/10.1016/j.fuel.2020.119553
16. Brokaw, R. S. Predicting transport properties of dilute gases. *Industrial & Engineering Chemistry Process Design and Development*, 1969, **8**(2), 240–253. https://doi.org/10.1021/i260030a015
17. Al-Harahsheh, M., Kingman, S., Saeid, A., Robinson, J., Dimitrakis, G., Alnawafleh, H. Dielectric properties of Jordanian oil shales. *Fuel Processing Technology*, 2009, **90**(10), 1259–1264. https://doi.org/10.1016/j.fuproc.2009.06.012

18. Jia, C., Li, J., Chen, J., Cui, S., Liu, H., Wang, Q. Simulation and prediction of co-combustion of oil shale retorting solid waste and cornstalk in circulating fluidized bed using CPFD method. *Applied Thermal Engineering*, 2020, **165**, 113574. https://doi.org/10.1016/j.applthermaleng.2019.03.145
19. Xiao, K. M., Wang, Y. M., Hu, H. B., Wen, Z., Lou, G. F., Su, F. Y. et al. Numerical analysis on heat transfer process in the coke oven with the multi-chamber coupling mathematical model. *Case Studies in Thermal Engineering*, 2023, **44**, 102858. https://doi.org/10.1016/J.CSITE.2023.102858
20. Huang, F. F., Liu, W. J., Chen, S. A., Tian, Z. X., Wei, J. T. Thermal desorption characteristics of the adsorbate in activated carbon based on a two-dimensional heat and mass transfer model. *Applied Thermal Engineering*, 2022, **214**, 118775. https://doi.org/10.1016/J.APPLTHERMALENG.2022.118775
21. Achenbach, E. Heat and flow characteristics of packed beds. *Experimental Thermal and Fluid Science*, 1995, **10**(1), 17–27. https://doi.org/10.1016/0894-1777(94)00077-L
22. Wakao, N., Kaguei, S. *Heat and Mass Transfer in Packed Beds*. Gordon and Breach Science Publishers, 1983.
23. Zhao, J. F., Sun, M. G., Zhang, L. X., Hu, C. Z., Tang, D. W., Yang, L. et al. Forced convection heat transfer in porous structure: effect of morphology on pressure drop and heat transfer coefficient. *Journal of Thermal Science*, 2021, **30**, 363–393. https://doi.org/10.1007/s11630-021-1403-x
24. Guo, W., Pan, J., Zhang, X., Deng, S., Zhu, C. Experimental and mechanistic study on isothermal oxidative pyrolysis of oil shale. *Journal of Analytical and Applied Pyrolysis*, 2023, **175,** 106215. https://doi.org/10.1016/J.JAAP.2023.106215
25. Baraj, E., Ciahotný, K., Hlinčík, T. The water gas shift reaction: catalysts and reaction mechanism. *Fuel*, 2021, **288**, 119817. https://doi.org/10.1016/j.fuel.2020.119817
26. Wei, J., Guo, Q., Song, X., Ding, L., Mosqueda, A., Liu, Y. et al. Effect of hydrothermal carbonization temperature on reactivity and synergy of co-gasification of biomass hydrochar and coal. *Applied Thermal Engineering*, 2021, **183**(P2), 116232. https://doi.org/10.1016/j.applthermaleng.2020.116232
27. Seberry, J. *Orthogonal Designs: Hadamard Matrices, Quadratic Forms and Algebras*. Cham, Springer, 2017.
28. Wang, C., Wang, C., Pan, H., Yue, Y. Effect of structure parameters on low nitrogen performance of burner based on orthogonal experiment method. *Case Studies in Thermal Engineering*, 2022, **39**, 102404. https://doi.org/10.1016/j.csite.2022.102404
29. Liu, W. Q. *Design of Experiments*. Tsinghua University Press, Beijing, 2020.
30. Ding, H., Liu, P., Chang, X., Zhang, B. A novel power quality comprehensive estimation model based on multi-factor variance analysis for distribution network with DG. *Processes*, 2023, **11**(8), 2385. https://doi.org/10.3390/pr11082385
31. Wu, Q. C. *Oil Shale Retorting Technology*. Liaoning Science and Technology Press, Shenyang, 2012.

Nomenclature

Symbol	Connotation	Unit
ε	Specific heat capacity of the solid	J kg^{-1} °C^{-1}
ρ	Density	kg/m^3
c_p	Specific heat capacity of the gas at constant pressure	J kg^{-1} °C^{-1}
t_f	Average temperature of the gas	°C
τ	Time	s
v	Velocity	m/s
λ_{feff}	Effective thermal conductivity of the gas	W m^{-1} °C^{-1}
λ_{seff}	Effective thermal conductivity of the solid	W m^{-1} °C^{-1}
$h_{v,s-f}$	Convective heat transfer coefficient per unit area between the gas and the solid phases	W m^{-2} °C^{-1}
t_s	Average temperature of the solids	°C
d_p	Particle diameter	mm
$_f$	Thermal conductivity of the gas	W m^{-1} °C^{-1}
u	Gas flow velocity	m s^{-1}
μ_f	Dynamic viscosity of the gas	Pa·s
$\phi_{go\text{-}in}$	Heat carried into the oxidation section by the gas mixture	W
$\phi_{go\text{-}out}$	Heat carried away from the oxidation section by the gas mixture	W
$\phi_{so\text{-}in}$	Heat carried into the oxidation section by the solids	W
$\phi_{so\text{-}out}$	Heat carried away from the oxidation section by the solids	W
ϕ_y	Heat released by the oxidation reaction in the oxidation sections	W
$m_{go,i-1}$	Mass flow rate of the gas mixture in model section i–1 of the oxidation section	kg s^{-1}
$m_{go,i}$	Mass flow rate of the gas mixture in model section i of the oxidation section	kg s^{-1}
$c_{go,i-1}$	Constant-pressure specific heat capacity of the gas mixture in model section i–1of the oxidation section	J kg^{-1} °C^{-1}
$c_{go,i}$	Constant-pressure specific heat capacity of the gas mixture in model section i of the oxidation section	J kg^{-1} °C^{-1}

Continued on the next page

Continued

Symbol	Connotation	Unit
$c_{so,i+1}$	Constant-pressure specific heat capacity of the solids in model section i+1 of the oxidation section	J kg^{-1} °C^{-1}
$c_{so,i}$	Constant-pressure specific heat capacity of the solids in model section i of the oxidation section	J kg^{-1} °C^{-1}
$t_{go,i-1}$	Average temperature of the gas mixture in model section i–1 of the oxidation section	°C
$t_{go,i}$	Average temperature of the gas mixture in model section i of the oxidation section	°C
$t_{so,i}$	Average temperature of the solids in model section i of the reduction section	°C
$t_{so,i+1}$	Average temperature of the solids in model section i+1 of the reduction section	°C
$h_{o,i}$	Heat transfer coefficient per unit area between the solids and the gas mixture in model section i of the oxidation section	W m^{-2} °C^{-1}
V	Heat transfer volume of the material layer in each model section	m^3
$m_{so,i+1}$	Mass flow rate of the solids in model section i+1 of the oxidation section	kg s^{-1}
$m_{so,i}$	Mass flow rate of the solids in model section i of the oxidation section	kg s^{-1}
$\phi_{gr\text{-}in}$	Heat carried into the reduction section by the gas mixture	W
$\phi_{gr\text{-}out}$	Heat carried away from the reduction section by the gas mixture	W
$\phi_{sr\text{-}in}$	Heat carried into the reduction section by the solids	W
$\phi_{sr\text{-}out}$	Heat carried away from the reduction section by the solids	W
ϕ_h	Heat absorbed by the reduction reaction in the reduction section	W
$m_{gr,j-1}$	Mass flow rate of the gas mixture in model section j–1 of the reduction section	kg s^{-1}
$m_{gr,j}$	Mass flow rate of the gas mixture in model section j of the reduction section	kg s^{-1}
$c_{gr,j-1}$	Constant-pressure specific heat capacity of the gas mixture in model section j–1of the reduction section	J kg^{-1} °C^{-1}
$c_{gr,j}$	Constant-pressure specific heat capacity of the gas mixture in model section j of the reduction section	J kg^{-1} °C^{-1}
$c_{sr,j+1}$	Constant-pressure specific heat capacity of the solids in model section j+1 of the reduction section	J kg^{-1} °C^{-1}

Continued on the next page

Continued

Symbol	Connotation	Unit
$c_{sr,j}$	Constant-pressure specific heat capacity of the solids in model section j of the reduction section	J kg^{-1} °C^{-1}
$t_{gr,j-1}$	Average temperature of the gas mixture in model section j–1 of the reduction section	°C
$t_{gr,j}$	Average temperature of the gas mixture in model section j of the reduction section	°C
$t_{sr,j}$	Average temperature of the solids in model section j of the reduction section	°C
$t_{sr,j+1}$	Average temperature of the solids in model section j+1 of the reduction section	°C
$h_{r,j}$	Heat transfer coefficient per unit area between the solids and the gas mixture in model section j of the reduction section	W m^{-2} °C^{-1}
$m_{sr,j+1}$	Mass flow rate of the solids in model section j+1 of the reduction section	kg s^{-1}
$m_{sr,j}$	Mass flow rate of the solids in model section j of the reduction section	kg s^{-1}
$\phi_{chc\text{-}in}$	Heat carried into the retorting section by the circulating heat-carrying gas	W
$\phi_{\text{gt-in}}$	Heat carried into the retorting section by the gas mixture	W
$\phi_{\text{gt-out}}$	Heat carried away from the retorting section by the gas mixture	W
$\phi_{\text{st-in}}$	Heat carried into the retorting section by the solids	W
$\phi_{st\text{-}out}$	Heat carried away from the retorting section by the solids	W
ϕ_{t}	Pyrolysis reaction heat in the retorting section	W
$\phi_{\text{g–t}}$	Heat consumed for retort gas to reach the gas mixture temperature in the retorting section	W
$m_{gt,k-1}$	Mass flow rate of the gas mixture in model section k–1 of the retorting section	kg s^{-1}
$m_{gt,k}$	Mass flow rate of the gas mixture in model section k of the retorting section	kg s^{-1}
$c_{gt,k-1}$	Constant-pressure specific heat capacity of the gas mixture in model section k–1of the retorting section	J kg^{-1} °C^{-1}
$c_{gt,k}$	Constant-pressure specific heat capacity of the gas mixture in model section k of the retorting section	J kg^{-1} °C^{-1}
$c_{st,k+1}$	Constant-pressure specific heat capacity of the solids in model section k+1 of the retorting section	J kg^{-1} °C^{-1}

Continued on the next page

Continued

Symbol	Connotation	Unit
$c_{st,k}$	Constant-pressure specific heat capacity of the solids in model section *k* of the retorting section	J kg^{-1} °C^{-1}
$t_{gt,k-1}$	Average temperature of the gas mixture in model section *k*–1 of the retorting section	°C
$t_{gt,k}$	Average temperature of the gas mixture in model section *k* of the retorting section	°C
$t_{st,k}$	Average temperature of the solids in model section *k* of the retorting section	°C
$t_{st,k+1}$	Average temperature of the solids in model section *k*+1 of the retorting section	°C
$h_{t,k}$	Heat transfer coefficient per unit area between the solids and the gas mixture in model section *k* of the retorting section	W m^{-2} °C^{-1}
$m_{st,k+1}$	Mass flow rate of the solids in model section *k*+1 of the retorting section	kg s^{-1}
$m_{st,k}$	Mass flow rate of the solids in model section *k* of the retorting section	kg s^{-1}
ϕ_{w}	Latent heat of moisture evaporation in the drying section	W
$\phi_{gd\text{-}in}$	Heat carried into the drying section by the gas mixture	W
$\phi_{gd\text{-}out}$	Heat carried away from the drying section by the gas mixture	W
$\phi_{sd\text{-}in}$	Heat carried into the drying section by the solids	W
$\phi_{sd\text{-}out}$	Heat carried away from the drying section by the solids	W
ϕ_{g-w}	Heat consumption for water vapor to reach the temperature of the mixed gas in the drying section	W
$m_{gd,m-1}$	Mass flow rate of the gas mixture in model section *m*–1 of the drying section	kg s^{-1}
$m_{gd,m}$	Mass flow rate of the gas mixture in model section *m* of the drying section	kg s^{-1}
$c_{gd,m-1}$	Constant-pressure specific heat capacity of the gas mixture in model section *m*–1 of the drying section	J kg^{-1} °C^{-1}
$c_{gd,m}$	Constant-pressure specific heat capacity of the gas mixture in model section *m* of the drying section	J kg^{-1} °C^{-1}
$c_{sd,m+1}$	Constant-pressure specific heat capacity of the solids in model section *m*+1 of the drying section	J kg^{-1} °C^{-1}
$c_{sd,m}$	Constant-pressure specific heat capacity of the solids in model section *m* of the drying section	J kg^{-1} °C^{-1}

Continued on the next page

Continued

Symbol	Connotation	Unit
$t_{gd,m-1}$	Average temperature of the gas mixture in model section m–1 of the drying section	°C
$t_{gd,m}$	Average temperature of the gas mixture in model section m of the drying section	°C
$t_{sd,m}$	Average temperature of the solids in model section m of the drying section	°C
$t_{sd,m+1}$	Average temperature of the solids in model section m+1 of the drying section	°C
$h_{d,m}$	Heat transfer coefficient per unit area between the solids and the gas mixture in model section m of the drying section	W m^{-2} °C^{-1}
$m_{sd,m+1}$	Mass flow rate of the solids in model section m+1 of the retorting section	kg s^{-1}
$m_{sd,m}$	Mass flow rate of the solids in model section m of the retorting section	kg s^{-1}
m_{w}	Mass flow rate of water vapor evaporated from the solids in the drying section	kg s^{-1}
$c_{w,m}$	Constant-pressure specific heat capacity of the water vapor in model section m of the drying section	J kg^{-1} °C^{-1}
$t_{a,m}$	Initial average temperature of the water vapor in model section m of the drying section	°C
$\vec{C}$	Vector comprising heat of the pyrolysis reaction and latent heat of evaporation of water (does not include temperature variables)	
$\vec{t}_1$	Vector comprising average temperatures of oil shale and gas in each modeled section	
$m_{y,all}$	Mass flow rate of gases generated by oxidative combustion in the oxidation section	kg s^{-1}
$m_{h,all}$	Mass flow rate of gases generated by the water-gas reaction in the reduction section	kg s^{-1}
m_{rws}	Mass flow rate of hot recycle gas introduced into the retorting section	kg s^{-1}
$m_{t,all}$	Mass flow rate of retort gas generated in the retorting section	kg s^{-1}
$m_{w,all}$	Mass flow rate of water vapor generated in the drying section	kg s^{-1}